Research on the Effect of Pouring Temperature on Hot-Tear Susceptibility of A206 Alloy by Simulation

MOHAMAD REZA NASRESFAHANI and MOHAMAD JAVAD RAJABLOO

Cast alloys with wide solidification ranges are prone to hot tearing. This study deals with prediction of hot tearing location and its intensity by computer simulation. The simulation was performed at different pouring temperatures on A206 aluminum alloy. As superheat increases, the critical fraction solid time increases which means the alloy is more susceptible to hot tearing. These theoretical predictions are in complete accordance with experimental results.

DOI: 10.1007/s11663-014-0100-5

I. INTRODUCTION

BEING the subject of metallurgical researches since 1940s, hot-tear defects still impose huge expenses to casting industries. Both ferrous and nonferrous alloys, especially those having a wide mushy zone, are susceptible to these defects.[1–3]

Hot tearing, also referred to as hot cracking, hot shortness, super solidus cracking, and shrinkage brittleness, is a tear which occurs during solidification of molten alloys while there is still some remaining melt between dendrites.[4] Hot tearing occurs in the last stages of solidification, in areas without sufficient feed metal. When the solid fraction is close to unity, tensile strains or contraction stresses arise in the ''mushy zone'' of the casting.[5,6]

In order to study the hot tearing of cast alloys in most methods, including the Ring test and the Dog bone test,[7–9] visual observation of castings followed by measuring the dimensions of the tears after solidification is necessary. However, none of these methods are accurate and reliable regarding their possible errors in detection and measurement of the lengths of the tears. They cannot also distinguish between the influences of different features on the occurrence of hot tearing. Recently, developed methods use load-measuring equipments,[10,11] including ultrasonic waves, X-ray microtomography, and *in situ* observations, to evaluate the hot tearing.[4,12–15] However, analysis of their complex output data is a difficult task.

Different factors, including the alloy composition, casting geometry and design, mold and core material, core design, and superheat, can influence the hot-tear susceptibility.[16] Although the proposed criteria are all quantified, they can only assess hot-tear susceptibility in limited (experimental) conditions. Moreover, some of the proposed methods require a special sample.

MOHAMAD REZA NASRESFAHANI, Lecturer, and MOHAMAD JAVAD RAJABLOO, Student, are with the Department of Materials Engineering, Najafabad Branch, Islamic Azad University, Najafabad, Iran. Contact e-mail: mr_nasr2001@ma.iut.ac.ir

Manuscript submitted January 16, 2014.
Article published online June 18, 2014.

For example, the hot tearing criterion proposed by Clyne and Davies[17] is based on the assumption that at the last stage of freezing it is difficult for the liquid to move freely, so liquid mass feeding cannot accommodate the strains developed during this stage. The last stage of freezing is considered as the most susceptible to hot tearing in this criterion. The tearing susceptibility coefficient is defined by the ratio of the vulnerable time period where hot tearing may develop, $(t_{0.99} - t_{0.9})$, and time available for the stress relief process where mass feeding and liquid feeding occur, $(t_{0.9} - t_{0.4})$. Where $t_{0.99}$ is the time when the volume fraction of solid, f_s, is 0.99, $t_{0.9}$ is the time when f_s is 0.9, and $t_{0.4}$ is the time when f_s is 0.4. Therefore, the cracking susceptibility coefficient HCS reads

$$\mathrm{HCS} = \frac{t_{0.99} - t_{0.9}}{t_{0.9} - t_{0.4}} \quad [1]$$

For using this criterion, we must determine solid fraction and its time by thermal analysis methods or simulation.

Another criterion for the hot tears is proposed by Rappaz *et al.*[18] Based upon a mass balance performed over the liquid and solid phases, it accounts for the tensile deformation of the solid skeleton perpendicular to the growing dendrites and for the induced interdendritic liquid feeding.

These methods and criteria[19,20] might be able to reduce the difficulties in determination of hot tearing but simulation and modeling still have priorities over them due to their speed and simplicity. In casting industries, simulations are applied extensively to understand the aspects of heat transfer and fluid transport phenomena as well as their influence on the microstructure, forming defects and occasionally the mechanical properties.[21]

By using the proper simulation software, the system equations can be solved and the location and severity of hot tearing can be predicted. For example, Pokorny *et al.*[22] used a new model to predict hot tears in a magnesium alloy permanent mold casting. The model calculates deformation and material damage. Preliminary estimates of temperature and strain rate-dependent mechanical properties were obtained from stress–strain

data. Simulations were performed of experimental test castings. The simulation results corroborate that the hot tears form most likely at the junction between the horizontal bar and the vertical sprue. The simulation results also confirm that hot tear susceptibility decreases with increasing mold temperature.

The aim of the present study is to investigate the influence of superheat on hot-tear susceptibility of A206 aluminum alloy, using the Procast software. To do this, a T-shaped model and mold with similar dimensions to References 23, 24 were used and the hot-tear indicator was applied to this model by Procast software. The results of the simulations were then compared and validated by experimental results.

The A206 alloy is a heat treatable engineering aluminum alloy used in applications where superior mechanical properties as well as light weight are needed. Its high strength, both at room and elevated temperatures, is achieved because of its higher levels of copper and lower levels of silicon contents. Despite the advantages, the presence of 4.2 to 5.0 pct copper has provided a wide solidification range for the alloy which puts it among one of the most susceptible alloys to hot tearing.[25]

II. MATERIALS AND METHODS

This study is based on finding out hot-tear susceptibility by using computer simulation. The results are then compared by those obtained from the experiments. To do this, the Procast simulation software which is a finite element software was selected. The Alloy used in this study is an Al-Cu alloy (A206) which is susceptible to hot tearing and has many applications in the aerospace industry. In Table I chemical composition of the A206 alloy is presented.[26]

The model selected for this study is a T-shaped model with dimensions and specifications presented in Figure 1. The T-shaped model makes it possible to apply stress and temperature on the desired point (T-junction).[4,24]

The T-shaped model and its sodium silicate bonded silica sand mold were inserted in the Procast software after designation. Thermodynamic and stress conditions of the alloy were set by the software. The boundary conditions including pouring temperature and heat transfer coefficient between the casting and the mold were then set.

In the experimental conditions, there are two steel bolts (hooks) to restrain the casting contraction at the end of the arms. These bolts are fixed to a load cell and two solid plates. During solidification, these bolts can prevent the release of tension and thus the stress is concentrated in the center of the sample (T-junction). Therefore, the end of each arm was considered as rigid and motionless during simulation. The hot tearing indicator was applied to the model. In order to examine the effect of pouring temperature (superheat) on hot-tear susceptibility, different pouring temperatures of 948 K, 973 K, 1023 K, and 1073 K (675 °C, 700 °C, 750 °C, and 800 °C) were respectively applied to the model. The results of the simulations were then compared to experimental results obtained through Reference 23.

III. RESULTS AND DISCUSSION

A. *Hot Tearing Indicator*

The constitutive model used to describe the material's behavior in the semi-solid state is the Gurson model which was developed to study the progressive micro-rupture through nucleation and growth of micro-voids. When the material is considered as elastic–plastic, the yielding condition in the Gurson model would be as the following[21]:

$$\phi(\sigma, x, T, \bar{\varepsilon}^{\mathrm{p}}, G_{\mathrm{u}}) = F(\sigma) - G_{\mathrm{u}}(\sigma, \bar{\varepsilon}^{\mathrm{p}}, f_{\mathrm{v}})k(, \bar{\varepsilon}^{\mathrm{p}}, T) = 0, \quad [2]$$

where $F(\sigma) = (3(s-X) : (s-X)/2)^{1/2}$is the Mises stress in terms of the deviatoric stress $S = \sigma - (tr\sigma)I/3$, κ represents the plastic flow stress due to isotropic hardening, and x denotes back stress due to kinematic hardening. The accumulated effective plastic strain is written as[21]

$$\bar{\varepsilon}^{\mathrm{p}} = \int_0^t \sqrt{(2/3)\,\overset{\circ}{\varepsilon}{}^{\mathrm{p}} : \overset{\circ}{\varepsilon}{}^{\mathrm{p}}}\,\mathrm{d}\tau, \quad [3]$$

with

$$\overset{\circ}{\varepsilon}{}^{\mathrm{p}} = \overset{\circ}{\gamma}\frac{\partial \phi}{\partial \sigma} \quad [4]$$

and $\overset{\circ}{\gamma}$ being the plastic flow parameter. The Gurson coefficient G_{u} is defined as

$$G_{\mathrm{u}} = -2f^{*}q_1 \cosh\left(\frac{tr(\sigma)}{2k} + \{1 + (q_1 f^{*})^2\}\right) \quad [5]$$

In which, q_1 is a material constant and

$$\begin{aligned} f^{*} &= f_{\mathrm{v}} \quad \text{for } f_{\mathrm{v}} \le f_{\mathrm{C}} \\ f^{*} &= f_{\mathrm{C}} + \frac{f_{\mathrm{u}} - f_{\mathrm{C}}}{f_{\mathrm{F}} - f_{\mathrm{C}}}(f_{\mathrm{v}} - f_{\mathrm{C}}) \quad \text{for } f_{\mathrm{v}} \ge f_{\mathrm{C}}, \end{aligned} \quad [6]$$

where $f_{\mathrm{u}} = 1/q_1 f_{\mathrm{c}}$ is the critical void volume fraction and f_{F} is the failure void volume fraction. Following Tvergaard and Needleman, their values are chosen as

Table I. Chemical Composition of the A206 Alloy

Cu	Mn	Mg	Ti	Si	Fe	Al	Elements
4.2 to 5	0.2 to 0.5	0.15 to 0.35	0.15 to 0.3	<0.05	<0.1	balance	standard percent

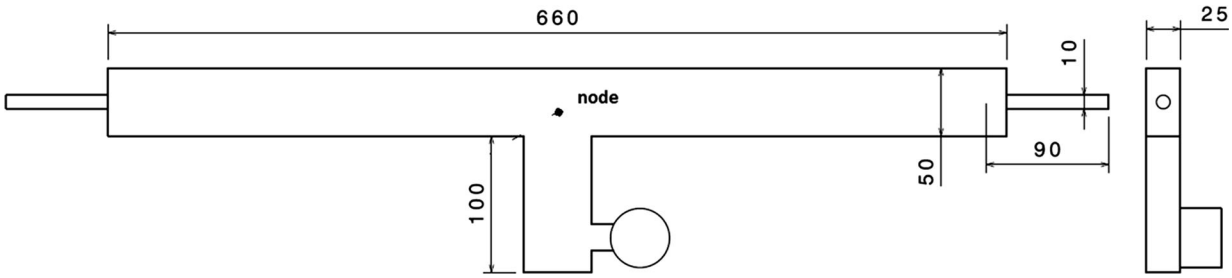

Fig. 1—Dimensions of the used T-shaped model.

$q_1 = 1.5$, $f_c = 0.15$, and $f_F = 0.25$. The Gurson coefficient characterizes the rapid loss of material's strength due to the growth of void's volume fraction f_v. When $f_v = f_F$ and for zero stress, *i.e.*, when the stress carrying capacity of the material vanishes, $f^* = f_u = 1/q_1$, and $G_u = 0$. The evolution of the void's volume fraction is described by the nucleation of new voids and the growth of existing voids, *i.e.*,

$$\dot{f}_v = \dot{f}_{\text{nucleation}} + \dot{f}_{\text{growth}} \quad [7]$$

, with the rate of void's growth defined as

$$\dot{f}_{\text{growth}} = (1 - f^*)tr\left(\overset{\circ}{\varepsilon}^p\right) = \overset{\circ}{\gamma}(1 - f^*)\left(\frac{3f^* q_1}{k}\right)\sinh\left(\frac{tr(\sigma)}{2k}\right) \quad [8]$$

$$\dot{f}_{\text{nucleation}} = \dot{e}_{ht} \quad [9]$$

$$e_{ht} = \int_{t_C}^{t} \sqrt{(2/3)\,\overset{\circ}{\varepsilon}^p : \overset{\circ}{\varepsilon}^p}\, d\tau \quad t_C \le t \le t_S, \quad [10]$$

where e_{ht} is defined as hot tearing indicator, t_c and t_s represent the time at coherency temperature and at solidus temperature, respectively.[21] It is observed that the hot tearing indicator is in fact the accumulated plastic strain in the semi-solid region which corresponds to the void's nucleation.

B. *Solid fraction*

Figure 2 shows the solid fraction graph gained from the simulated model poured at 948 K (675 °C). This graph denotes the temperature node at the center of the T-shaped model (T-junction). This node represents the hot tearing area of experimental samples, and its position is shown in Figure 1. We can see in the node that after 337 seconds the solid fraction reaches 1. Therefore, this time represents the end of solidification at the node. This time reaches 487 seconds in the model poured at 1073 K (800 °C). The end of solidification times of the remaining models with pouring temperatures of 973 K and 1023 K (700 °C and 750 °C) are 354 and 427 seconds, respectively (Table II). Solid fractions between 0.9 and 0.99 are considered as critical. The hot-tear susceptibility would increase when the time

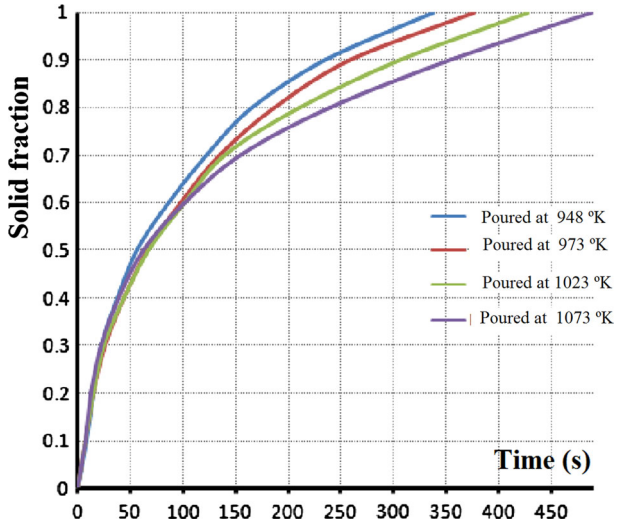

Fig. 2—Solid fraction graph.

exposed in critical solid fractions increases. In the model poured at 948 K (675 °C), the exposure time in critical solid fraction is about 83 seconds and for the model poured at 1073 K (800 °C), this time is increased to 125 seconds. As a result, the hot-tear susceptibility increases. This theory is in accordance with the experimental results presented in Section III–C.

C. *Cooling and Porosity Distribution*

Figure 3 represents the solidification time at different parts of the models with different pouring temperatures. As can be seen, in the model with lower superheat (Figure 3(a)), solidification starts at the end of the arms and moves toward the center of the model. A high difference exists between the solidification times of different parts of this model and the model has skin-type solidification.

According to Figure 4(a) in this kind of solidification, shrinkage defects and porosities concentrate in the center of the model. Experimental studies show that when porosity concentrates in the center of the sample, the surface above the porous area collapses (Figure 5(a)). For the sample poured at higher temperature, the solidification times of different parts are less different. Therefore, this difference is the least for the model poured at 1073 K (800 °C) (Figure 3(d)) and the

Table II. Time of Different Solid Fractions and HCS Parameters was Computed for Each Pouring Temperature

Pouring Temperature [K (°C)]	The Time When f_s is 0.4 (s)	The Time When f_s is 0.9 (s)	The time When f_s is 0.99 (s)	HCS
948 (675)	36	246	329	0.395
973 (700)	40	262	350	0.396
1023 (750)	43	307	423	0.439
1073 (800)	47	356	481	0.404

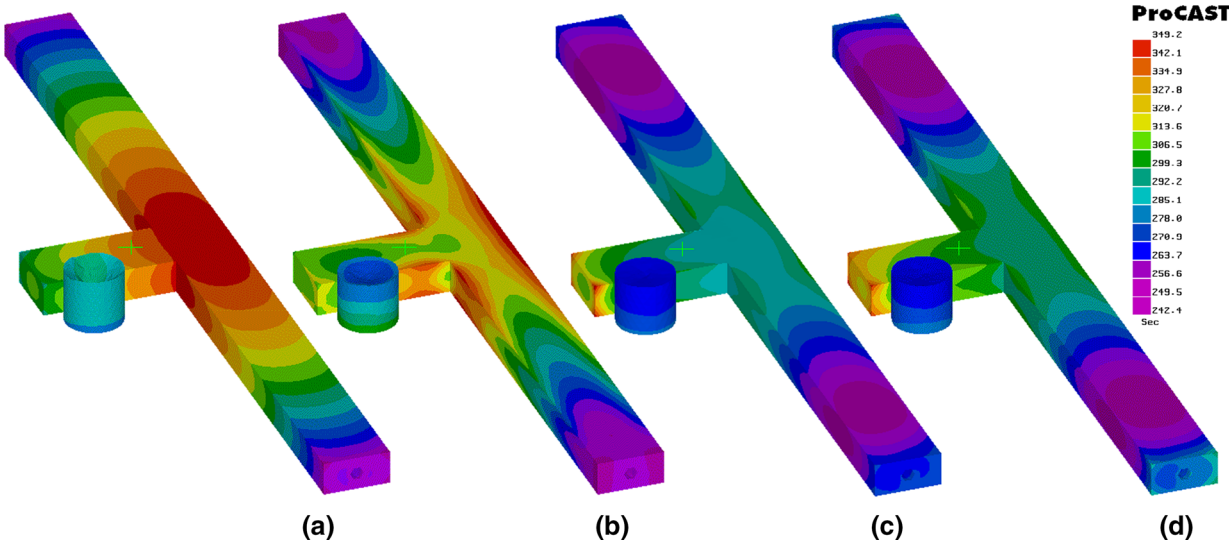

Fig. 3—Solidification time, (*a*) poured at 948 K (675 °C), (*b*) poured at 973 K (700 °C), (*c*) poured at 1023 K (750 °C), (*d*) poured at 1073 K (800 °C).

mushy solidification occurs as a result of the increase in solidification time. According to Figure 4(d), the volume of shrinkage porosity has increased by increasing the pouring temperature but its distribution in all parts of the model is uniform. It seems like in the model with lower pouring temperature, the hot tearing tendency increases due to the concentration of defects in the center. But this is not true. In fact, by decreasing the superheat, directional solidification occurs. As a result, the contraction of solidified parts is supported by the melt in the center of the sample. So in final stages, when the hot spot in the center of the sample is solidifying, it is not subjected to any significant shrinkage stress (according to Figure 6) which means that no tear would occur between the dendrites. Figure 6 represents the stress distribution at different parts of the models with different pouring temperatures. According to Figure 6 in the skin-type solidification [model poured at 948 K (675 °C)], the maximum stress in the hot spot (T-Junction) is about 13 MPa whereas in the mushy solidification [model poured at 1073 K (800 °C)] maximum stress in the hot spot is more than 18 MPa. In the skin-type solidification, a large portion of shrinkage compensates by liquid. But in the mushy solidification, shrinkage cannot compensate therefore volume reduction appears as a porosity or residual stress.

For the occurrence of hot tearing, stress should be focused on the hot spot when this area is mushy. In the Mushy solidification, hot spat area remains mushy for more time. Therefore, if concluded that hot-tear susceptibility increases by increasing the pouring temperature, it is true.

D. *Validation*

Validation of this study is corroborated experimentally. Simulation results were compared with the experimental results in Reference 13 and their accuracy was assessed. Figure 5(a) shows the macroscopic image of the center of the sample poured at 948 K (675 °C). There are tiny cracks in the area, shown by a white circle. This implies a low susceptibility to hot tearing of the poured sample at 948 K (675 °C). Figure 5(e) shows the simulation result (from Eq. [10]) for this sample. The software has predicted this area precisely as a real sample.

Figures 5(b) and (f) show the macroscopic image of the center of the sample poured at 973 K (700 °C) and the simulation of the hot tearing susceptibility of the sample, respectively. In this case, there can be seen a good match between the simulation and experimental results. Figure 5(c) shows the macroscopic image from the center of the sample poured at 1023 K (750 °C). Comparison of the hot tearing severity in this sample with simulation results shows that hot tearing susceptibility has increased by increasing the superheat. Note that in Figure 5, the software shows an increase in hot tearing susceptibility when developing the hot tearing

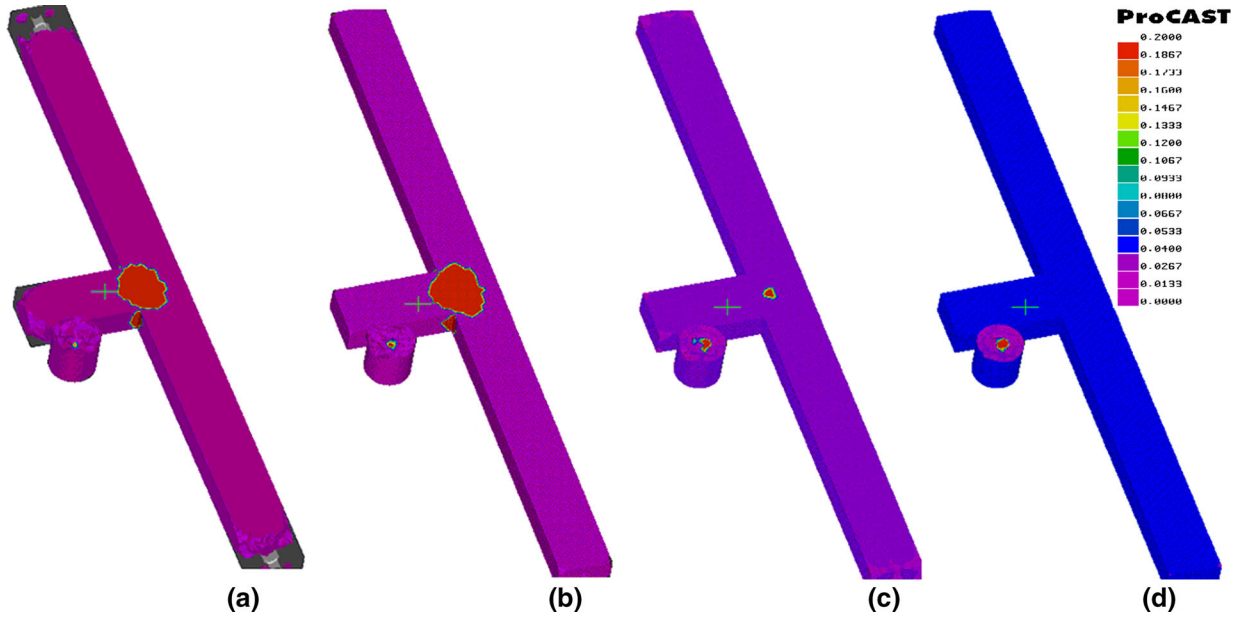

Fig. 4—Shrinkage porosity, (*a*) poured at 948 K (675 °C), (*b*) poured at 973 K (700 °C), (*c*) poured at 1023 K (750 °C), (*d*) poured at 1073 K (800 °C).

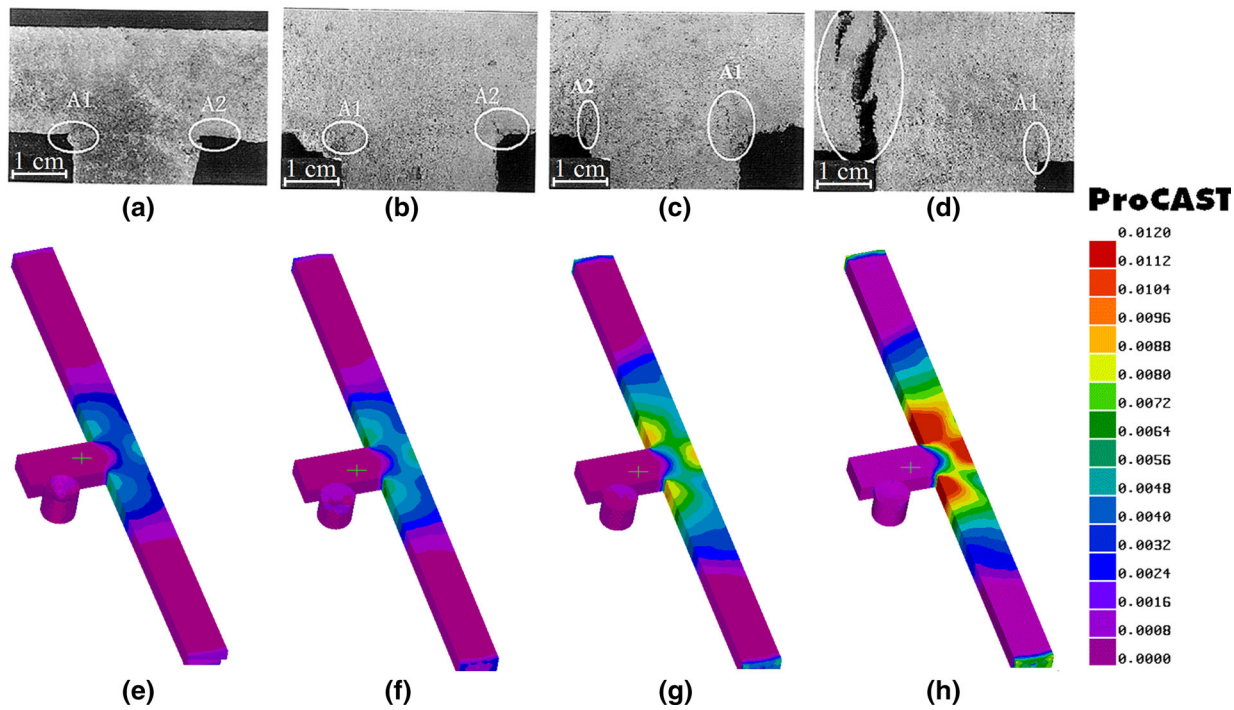

Fig. 5—Simulation hot tearing susceptibility and experimental results of samples (*a* and *e*) poured at 948 K (675 °C), (*b* and *f*) poured at 973 K (700 °C), (*c* and *g*) poured at 1023 K (750 °C) and (*d* and *h*) poured at 1073 K (800 °C).

area. The results presented in the previous section confirm the increasing risk of hot tearing by increasing superheat. The severity of hot tearing in the sample poured at 1073 K (800 °C) is maximum in both experimental and simulation results. Hot-tear susceptibility in this sample is severely high and can cause the left arm to be separated (Figure 5(d)). Simulation results (Figure 5(h)) show a significant increase in the susceptibility of hot tearing in this area.

For comparison, the effect of superheat on the hot tearing susceptibility of A206 alloy was examined through Clyne and Davies criterion. Required information for calculating hot tearing susceptibility extracted from cooling curves. This information is provided in

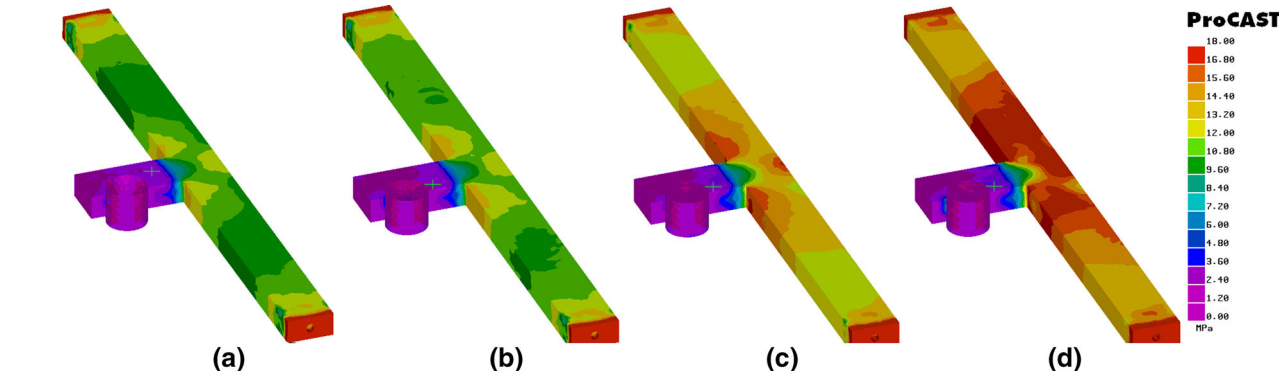

Fig. 6—Stress distribution at different parts of the models, (*a*) poured at 948 K (675 °C), (*b*) poured at 973 K (700 °C), (*c*) poured at 1023 K (750 °C), and (*d*) poured at 1073 K (800 °C).

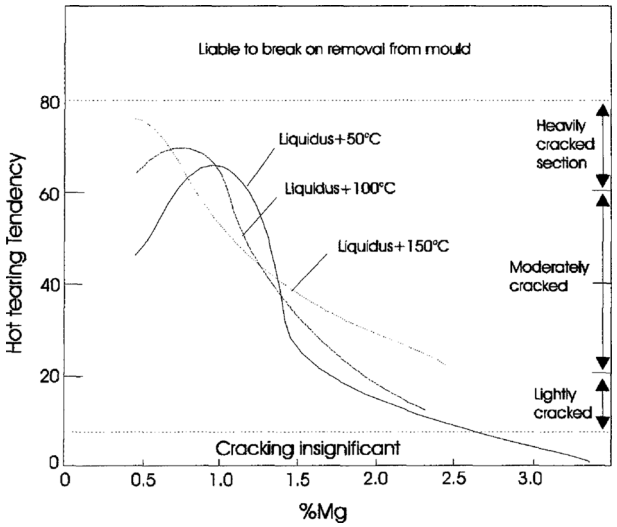

Fig. 7—Relationship between the degrees of hot tearing and melt superheat and Mg content in an Al-Mg alloy[27].

Table II. Then HCS parameter was computed for each pouring temperature. According to Table II, HCS value for model poured at 948 K (675 °C) is 0.395. HCS value increases by increasing the superheat, and for model poured at 1073 K (800 °C) this value is 0.404. This means that ratio of the vulnerable time period and time available for the stress relief process increased by increasing the super heat. So hot tear susceptibility increases by increasing the pouring temperature. In this case, there can be seen a good match between the simulation and HCS results.

Although the HCS is a simple criterion and its required information is readily available, but because of neglecting stress, it seems that this criterion is weak in some case.

These results are in complete accordance with prior results reported by Clyne and Davies.[27] They established a relationship between the degrees of tearing and melt superheat. Their results on Al-Mg alloys with different degrees of superheat are shown in Figure 7. It can be observed that when the superheat is high, the maximum value in hot tearing susceptibility curve is raised and moves to lower magnesium contents.

IV. CONCLUSIONS

In this study, the effect of superheat on the hot tearing susceptibility of A206 alloy was examined through simulation. It is shown that the exposure time in critical solid fraction is increased by increasing the pouring temperature. At higher pouring temperature, the solidification is mushy and the porosity spreads in the whole sample. On the other hand, hot-tear susceptibility of this sample increased as a result of the increase in the exposure time in critical solid fraction. At lower pouring temperatures, the model has skin-type solidification and the porosity is localized in the center. But contraction stress is not localized at this point. Therefore, hot-tear susceptibility is decreased. Simulation results showed that hot-tear susceptibility is increased by increasing the superheat. This was associated with the reduced cooling rate, increased exposure time at critical solid fraction, and a more localized hot spot formation at the center of the model. These results are in complete accordance with prior results reported. Hot tears observed in the experiments followed the same trend of damage, both in terms of location and severity, as predicted by simulation.

REFERENCES

1. J. Campbell: *Castings*, 2nd ed., Buttenvorth-Heinemann, Oxford, 2003, p. 130.
2. D.G. Eskin: *Physical Metallurgy of Direct Chill Casting of Aluminum Alloys*, 1st ed., Taylor & Francis, Boca Raton, 2008, p. 45.
3. J.B. Mitchell, S.L. Cockcroft, D. Viano, C. Davidson, and D. Stjohn: *Metall. Mater. Trans. A*, 2007, vol. 38A, pp. 2503–12.
4. C. Monroe and C. Beckermann: *Mater. Sci. Eng. A*, 2005, vols. 413–414, pp. 30–36.
5. A. Stangeland, A. Mo, M.M. Hamdi, D. Viano, and C. Davidson: *Metall. Mater. Trans. A*, 2006, vol. 37A, pp. 705–14.
6. Y. Turen: *Mater. Des.*, 2013, vol. 49, pp. 1009–15.

7. P.R. Beeley: *Foundry Technology*, 2nd ed., Butterworth-Heinemann, Oxford, 2001, p. 281.
8. J. Zhang and R.F. Singer: *Acta Mater*., 2002, vol. 20, pp. 1869–79.
9. L. Sweet, M. Easton, J. Taylor, J. Grandfield, C. Davidson, and L. Lu: *Metall. Mater. Trans. A*, 2012, vol. 44A, pp. 1–12.
10. M. Li, H. Wang, Z. Wei, and Z. Zhu: *Mater. Des*., 2010, vol. 31, pp. 2483–87.
11. Z. Wang, Y. Huang, A. Srinivasan, Z. Liu, F. Beckmann, K.U. Kainer, and N. Hort: *Mater. Des*., 2013, vol. 47, pp. 90–100.
12. M.O. Pekguleryuz, X. Li, and C.A. Aliravci: *Metall. Mater. Trans A*, 2009, vol. 40A, pp. 1436–56.
13. G. Cao and S. Kou: *AFS Trans*., 2007, vol. 115, pp. 709–20.
14. A.B. Phillion, S.L. Cockcroft, and P.D. Lee: *Mater. Sci. Eng. A*, 2008, vol. 491, pp. 237–47.
15. P.D. Grasso, J.M. Drezet, and M.Rappaz: *J. Met*., 2002.
16. Z. Lin, C. Monroe, R. Huff, and C. Beckermann: *Modeling of Casting. Welding and Advanced Solidification Processes-XII*, TMS, Warrendale, 2009.
17. T.W. Clyne and G.L. Davies: *Proceedings of the Conference on Solidification and Casting of Metals*, London, 1979, p. 274.
18. M. Rappaz, J.M. Drezet, and M. Gremaud: *Metall. Mater. Trans. A*, 1999, vol. 30A, p. 449.
19. D.G. Eskin and L. Katgerman: *Metall. Mater. Trans. A*, 2007, vol. 38A, pp. 1511–19.
20. Suyitno, W.H. Kool, and L. Katgerman: *Metall. Mater. Trans. A*, 2005, vol. 36A, pp. 1537–46.
21. J. Guo and J.Z. Zhu: *Proceedings of the 5th Decennial International Conference on Solidification Processing*, Sheffield, 2007.
22. M. Pokorny, C. Monroe, and C. Beckermann: *Int. J. Metalcast*., 2008, vol. 8, pp. 41–53.
23. M.R. Nasresfahani and B. Niroumand: *J. Mater. Charact*., 2010, vol. 61, pp. 318–24.
24. M.R. Nasresfahani and B. Niroumand: *Met. Mater. Int*., 2010, vol. 16, pp. 35–38.
25. W. Sequeria, V. Pikhovich, and D. Weiss: *Finding New Strength in Aluminum. Modern Casting*, 2006, pp. 38–41.
26. J.E. Hatch: *Aluminum Properties and Physical Metallurgy*, 1st ed., American Society for Metals, Metals Park, OH, 1984.
27. T.W. Clyne and G.J. Davies: *Br. Foundrym*., 1975, vol. 68, p. 238.